8-14-2018

Molecular Determinants of Substrate Specificity in Human Insulin-degrading Enzyme

Lazaros Stefanidis
Sacred Heart University, stefanidisl@sacredheart.edu

Nicholas D. Fusco
Sacred Heart University, fuscon29417@sacredheart.edu

Samantha E. Cooper
Fairfield University

Jilian E. Smith-Carpenter
Fairfield University

Benjamin J. Alper
Sacred Heart University, alperb@sacredheart.edu

Recommended Citation

Stefanidis, L., Fusco, N. D., Cooper, S. E., Smith-Carpenter, J., & Alper, B. J. (2018). Molecular determinants of substrate specificity in human insulin-degrading enzyme. *Biochemistry, 57*(32), 4903-4914. doi: 10.1021/acs.biochem.8b00474

Biochemistry

Article

Molecular determinants of substrate specificity in human insulin-degrading enzyme

Lazaros Stefanidis, Nicholas D. Fusco, Samantha E. Cooper, Jillian Smith-Carpenter, and Benjamin J. Alper

Biochemistry, **Just Accepted Manuscript** • DOI: 10.1021/acs.biochem.8b00474 • Publication Date (Web): 13 Jul 2018

ACS Publications

is published by the American Chemical Society. 1155 Sixteenth Street N.W., Washington, DC 20036

Molecular Determinants of Substrate Specificity in Human Insulin-Degrading Enzyme

Lazaros Stefanidis[1], Nicholas D. Fusco[1], Samantha E. Cooper[2], Jillian E. Smith-Carpenter[2] and Benjamin J. Alper[1]*

From the [1]Department of Chemistry, Sacred Heart University, Fairfield CT, USA 06825; [2]Department of Chemistry and Biochemistry, Fairfield University, Fairfield CT 06824

Running title: *Functional analysis of the IDE substrate binding interface*

*To whom correspondence should be addressed: Benjamin J. Alper: Department of Chemistry, Sacred Heart University, Fairfield CT 06825; alperb@sacredheart.edu; Tel. (203) 396-8105, Fax. (203) 371-7888.

Keywords: insulin-degrading enzyme, M16A metalloendopeptidase, insulin, amyloid peptide

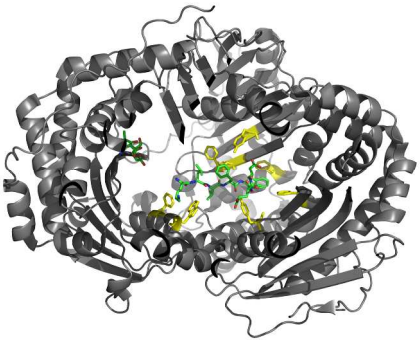

ABSTRACT

Insulin-degrading enzyme (IDE) is a 110 kDa chambered zinc metalloendopeptidase that degrades insulin, amyloid beta, and other intermediate-sized aggregation prone peptides that adopt β-structures. Structural studies of IDE in complex with multiple physiological substrates have suggested a role for hydrophobic and aromatic residues of the IDE active site in substrate binding and catalysis. Here, we examine functional requirements for conserved hydrophobic and aromatic IDE active site residues that are positioned within 4.5 Angstroms of IDE bound insulin B chain and amyloid beta peptides in the reported crystal structures for the respective enzyme-substrate complexes. Charge, size, hydrophobicity, aromaticity, and other functional group requirements for substrate binding IDE active site residues were examined through mutational analysis of the recombinant human enzyme and enzyme kinetic studies conducted using native and fluorogenic derivatives of human insulin and amyloid beta peptides. A functional requirement for IDE active site residues F115, A140, F141, Y150, W199, F202, F820, and Y831 was established, and specific contributions of residue charge, size and hydrophobicity in substrate binding, specificity, and proteolysis were demonstrated. IDE mutant alleles that exhibited enhanced or diminished proteolytic activity towards insulin or amyloid beta peptides and derivative substrates were identified.

INTRODUCTION

Human insulin-degrading enzyme (IDE; EC 3.4.24.56, GenBank reference sequence BC096336) is a 110 kDa chambered zinc metalloendopeptidase of the M16A subfamily. The enzyme is notable for its role in the proteolysis of several physiologically significant peptides that adopt β-structures, including insulin (1, 2), glucagon (3), amylin (4) and amyloid beta (Aβ) peptides (5).

Functional analysis of the IDE substrate binding interface

Multiple studies point to roles for IDE in metabolic signaling and disease. Consistent with a role for IDE within the insulin signaling pathway, human IDE polymorphisms have been associated with type 2 diabetes (6, 7), and in IDE deficient mouse models, loss of IDE corresponds with elevated serum insulin and glucose levels, and intolerance to glucose challenge after fasting (8, 9). Moreover, in accordance with the amyloid hypothesis, which asserts that variations in neuronal Aβ production and catabolism contribute to the development of Alzheimer's disease (10, 11, 12), IDE is thought to play a neuroprotective role in the clearance of free Aβ peptides (8, 13, 14, 15). Proteolytic clearance of Aβ peptides by IDE is hypothesized to limit peptide accumulation, plaque formation and neurotoxicity (16, 17, 18, 19). Consistent with this hypothesis, transgenic mice that overexpress amyloid precursor protein exhibit cognitive deficits, whereas neuronal levels of Aβ and premature death rates are significantly reduced in transgenic mice where IDE is overexpressed in parallel (20), and primary neurons cultured from IDE knockout mice show >90% reduction in the rate of Aβ degradation (8).

IDE is a member of the M16A subfamily of zinc metalloendopeptidases. M16A peptidases are broadly conserved, with homologs expressed throughout the prokaryotic and eukaryotic kingdoms (21, 22). M16A enzymes hydrolyze intermediate-sized (<10 kDa) peptides with propensity to adopt β-structures at multiple cleavage sites, breaking substrates into smaller fragments or component amino acids. Molecular determinants of substrate recognition by IDE have been examined previously (5, 17, 19, 23, 24). A distinguishing feature that is shared among IDE substrates is a common propensity to form β-structure interactions with the β6 strand of the IDE active site (23, 24). No absolute primary sequence requirement is recognized among IDE substrates (25). However, studies of rat IDE using synthetic fluorogenic peptides revealed preferential cleavage specificity on the amino side of bulky hydrophobic and basic residues and support the assignment of an extended substrate binding site (26, 27). Substrates of IDE and other M16A enzymes must be small enough to fit within the substrate binding chamber to facilitate proteolysis, and peptides with pronounced electropositive character at their carboxy-termini may be poor IDE substrates due to repulsive electrostatic interactions with the electropositive C-terminal face of the substrate binding chamber (23). In addition, larger IDE substrates also interact with IDE at one or more exosites, located as much as 30 Å or more from the catalytic center (23, 28, 29).

Structural data is available for IDE alone (30), as well as in complex with insulin, Aβ, amylin and glucagon (23, 31). Like other enzymes of the M16A subfamily, IDE adopts a structure analogous to that of a clamshell, with large (~50 kDa) N- and C-terminal domains positioned about a central cavity. The opening and closing of the N- and C- terminal domains is required to facilitate substrate access to the enzyme active site and may represent a rate limiting step within the IDE catalytic mechanism (23). The mode of substrate binding to the open IDE conformer has been recently elucidated by structural studies conducted using electron microscopy, suggesting that amyloidogenic peptides stabilize the disordered catalytic cleft, facilitating selective degradation through substrate-assisted catalysis (31). In the reported substrate bound closed crystal structures, IDE substrates are enclosed within a large (16,000 $Å^3$) central binding chamber, or "crypt". Herein, the catalytic Zn^{2+} ion is coordinated by residues of the invariant *HXXEH* (inverzincin) motif that is conserved among all M16 family proteases (21, 32, 33).

The IDE inverzincin motif includes several enzymatic residues that are critical for Zn^{2+} binding and catalysis (21, 32, 33) while the catalytic Zn^{2+} ion itself is positioned near an extended β-sheet that forms multiple contacts with substrates adopting β-strand conformations in the reported substrate bound IDE crystal structures (23). Within and around this substrate interfacing β-sheet, IDE contains several conserved hydrophobic and aromatic residues that are positioned in close proximity to hydrophobic regions of bound substrates with high β-propensity (23, 24). Substrate specificity of IDE and other M16A homologs has thus been proposed to depend on the character of hydrophobic and aromatic active site residues that are proximal to the catalytic zinc ion within the enzyme's central catalytic chamber (23). Yet, few experimental efforts have

sought to directly investigate specificity determinants of the IDE active site, and studies of IDE active site substrate specificity determinants using native IDE substrates or their derivatives are particularly lacking.

This study examines the molecular basis of substrate specificity of human IDE through mutational analysis of conserved hydrophobic and aromatic IDE active site residues positioned within 4.5 Å of insulin B chain and Aβ 1-40 in the substrate bound IDE crystal structures PDB ID 2G54 and PDB ID 2G47 (23). Purified bacterially expressed human IDE, recombinant insulin and Aβ peptides, and quenched fluorogenic (FRET) peptide derivatives thereof were used to probe the functional contributions of IDE active site residues in substrate recognition and proteolysis. We observe that conserved hydrophobic and aromatic residues of the IDE active site are critical for substrate binding and enzyme activity and report the identification of IDE mutant alleles that exhibit hyperactive proteolytic activity towards insulin or Aβ derivative FRET substrates, as well as IDE mutants that exhibit increased selectivity for proteolysis of insulin or Aβ peptides.

RESULTS

Identification of conserved hydrophobic and aromatic substrate interfacing residues of the IDE active site

The requirement for conserved hydrophobic and aromatic IDE active site residues within 4.5 Å of insulin B chain or Aβ 1-40 peptides in crystal structures PDB ID 2G54 and PDB ID 2G47 (23) was evaluated through kinetic study of recombinant human IDE mutants. Insulin, Aβ 1-40 and derivative quenched fluorogenic peptides that were developed for use in this study were applied to characterize the proteolytic activity of purified IDE *in vitro*. Conserved hydrophobic and aromatic IDE active site residues that were characterized by mutational and kinetic study are depicted in Figure 1.

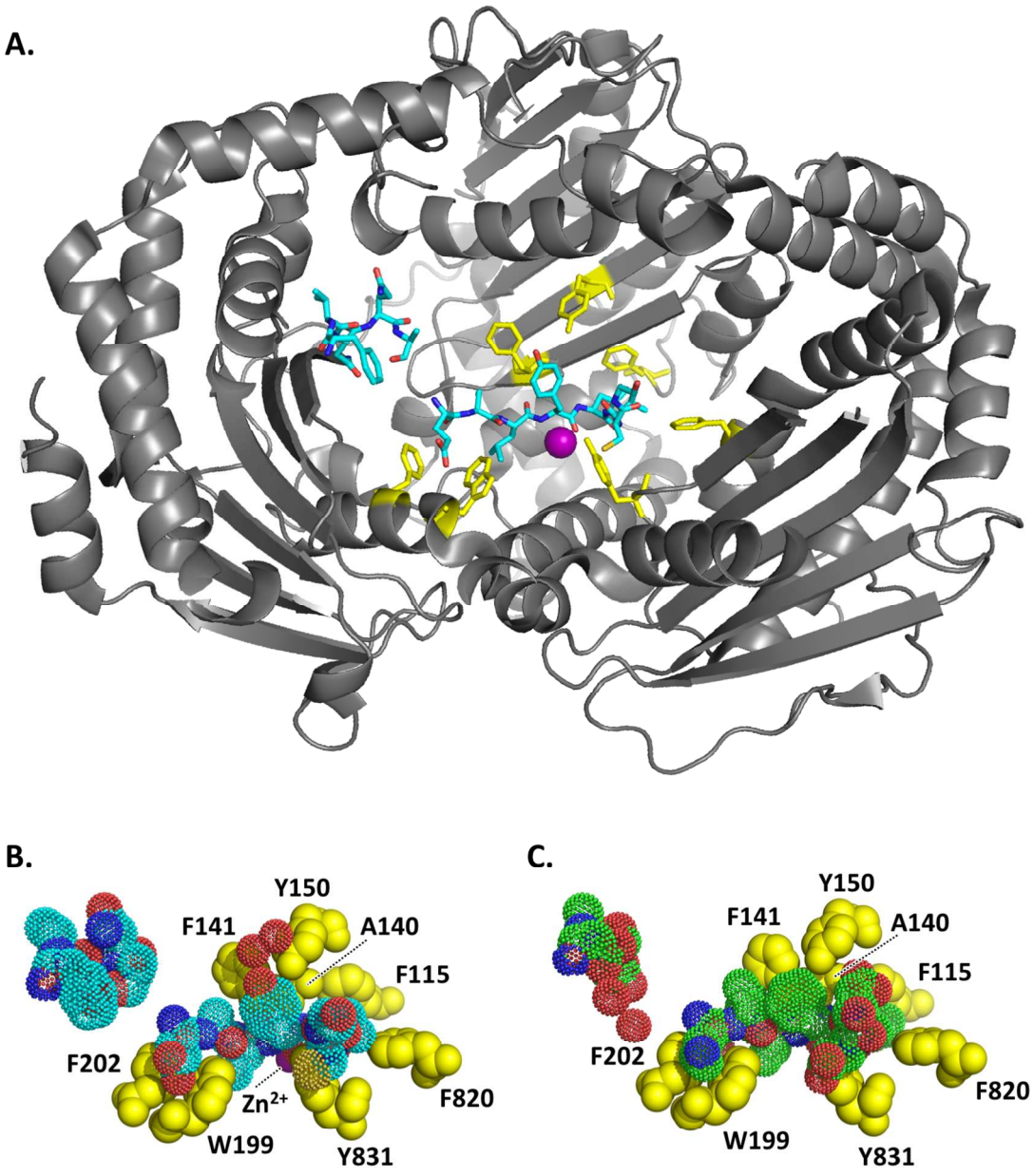

Figure 1. Conserved hydrophobic and aromatic substrate interfacing residues of the IDE active site. **A.** Structural model of IDE (grey ribbons) in complex with insulin B chain (main chain carbon atoms are represented by cyan sticks; positions of oxygen and nitrogen atoms are indicated in red and blue, respectively); this image has been adapted from structural coordinates reported in PDB ID 2G54 (23). Conserved hydrophobic and aromatic residues of the IDE active site that were subject to mutational analysis in this study are indicated (yellow sticks). In the perspective shown, exterior residues of IDE that obscure bound substrate have been rendered transparent to reveal the enzyme active site. **B.** Space-filling representation of IDE in complex with insulin B chain (23). Conserved hydrophobic and aromatic residues of the IDE active are represented as solid yellow spheres, with the region of defined electron density for insulin B chain shown in cyan (carbon atoms), blue (nitrogen), red (oxygen) and yellow (sulfur) punctate surfaces. The catalytic Zn^{2+} ion, partially occluded, is shown as a purple sphere. **C.** Space-filling representation of IDE in complex with Aβ 1-40 peptide (PDB ID 2G47). Regions of defined electron density for Aβ 1-40 carbon atoms are represented as green punctate surfaces.

Functional analysis of the IDE substrate binding interface

To examine specific functional group requirements for IDE active site residues, targeted mutagenic substitutions introduced amino acid residues with varying hydrophobicity, charge, size, and aromaticity in place of conserved hydrophobic and aromatic residues of the IDE active site. Targeted substitutions were introduced through inverse PCR amplification of the wild-type IDE expression construct (i.e., $IDE_{(M42\text{-}L1019)}$-6xHis; hereafter referred to as "WT IDE") using mutagenic oligonucleotide primers (Table S1). The proximity of IDE active site residues targeted by mutational analysis to regions of substrate electron density in the reported insulin B chain and Aβ 1-40 bound IDE crystal structures (23) is described in Table S2. Hydrogen atoms are omitted from structural representations and were not considered in calculations of residue proximity. All mutants characterized in this study were readily expressed and purified by immobilized metal affinity chromatography and were isolated as proteins of the expected molecular mass (Figure S1). A multiple sequence alignment of eukaryotic and prokaryotic IDE homologs, indicating the positions of active site residues that were targeted for mutagenesis within this study is presented in Figure S2.

Application of insulin B chain and Aβ derivative FRET substrates for real-time kinetic analysis of IDE proteolytic activity is presented in Figure 2. Addition of WT IDE but not the catalytically inactive (32) IDE E111Q mutant to proteolytic assays conducted using insulin B chain and Aβ derivative FRET substrates resulted in increased sample fluorescence over time (Figure 2A and 2B, respectively). For each substrate, a linear correlation between fluorescence intensity and peptide hydrolysis product concentration was established and was in turn used to inform kinetic parameters of IDE function (Figures 2C, 2D). The insulin B chain derivative FRET substrate Mca-VEALYLVCGEK(Dnp)-OH was bound by IDE with higher affinity yet was hydrolyzed more slowly than the Aβ derivative FRET substrate Mca-QKLVFFAEDVK(Dnp)-OH (K_{half} 1.26 ± 0.13 μM, k_{cat} 11.9 ± 0.7 min^{-1} vs. K_{half} 3.16 ± 0.69 μM, k_{cat} 34.3 ± 4.4 min^{-1}, respectively; Figure 2E, 2F and Table 1).

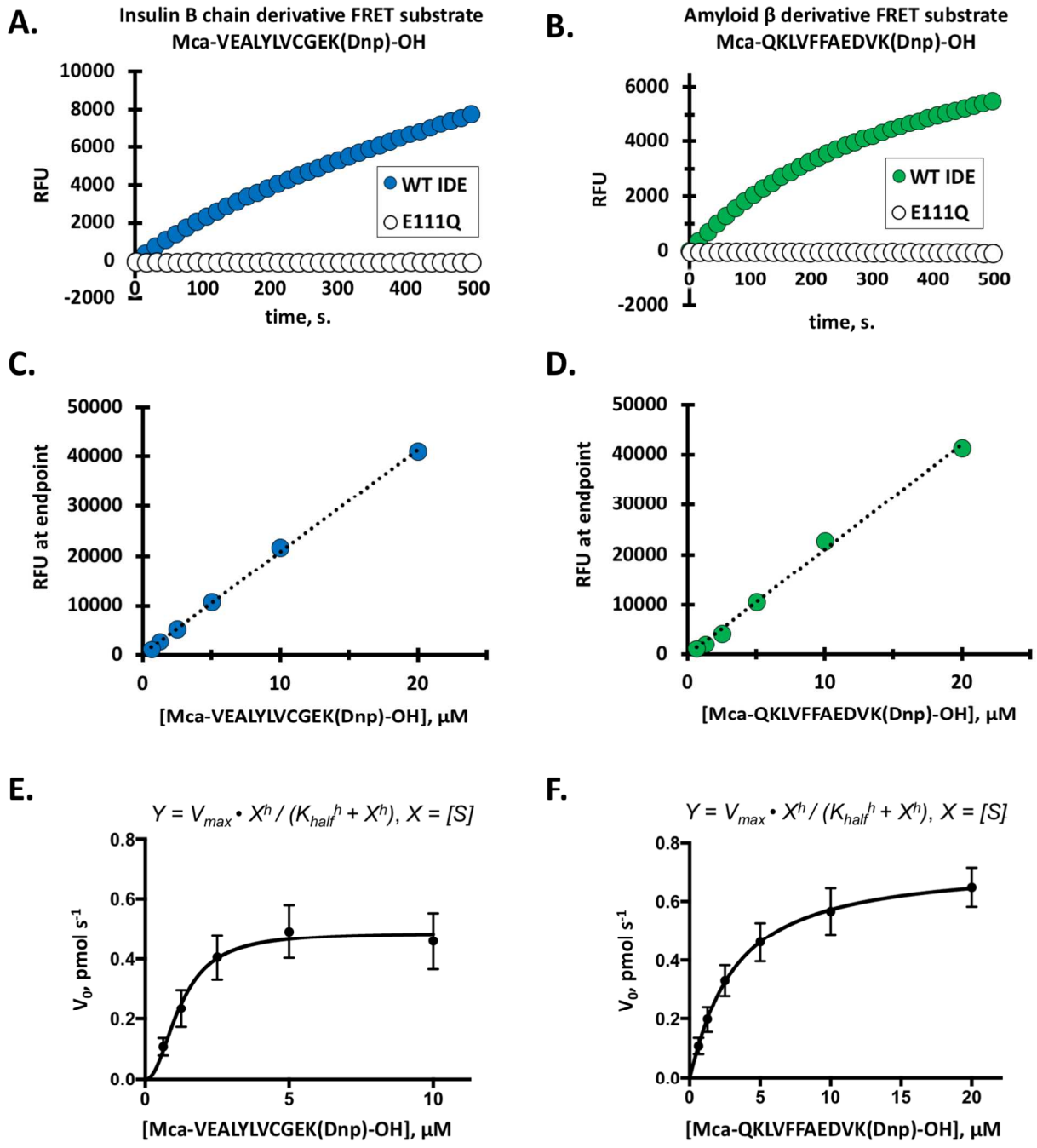

Figure 2. Insulin and Aβ derivative fluorogenic substrates for real-time kinetic analysis of IDE activity. A. Reaction progress curve for a representative kinetic IDE proteolysis assay conducted using insulin B chain derivative Mca-VEALYLVCGEK(Dnp)-OH FRET substrate and purified recombinant IDE. Sample fluorescence (Relative Fluorescence Units, RFU) is reported as a function of time (s). WT IDE, or the catalytically inactive IDE E111Q mutant (28), were added to the reaction mixture to initiate proteolysis, and fluorescence measurements were recorded at 15 s intervals (Excitation: 325 ± 25 nm, Emission: 420 ± 25 nm). **B.** Reaction progress curve from a representative kinetic assay conducted using the Aβ derivative fluorogenic substrate Mca-QKLVFFAEDVK(Dnp)-OH. **C.** Standardization of the fluorogenic assay. Sample fluorescence at endpoint is reported as a function of initial substrate concentration for the insulin B chain derivative Mca-VEALYLVCGEK(Dnp)-OH FRET peptide. **D.** Standardization of the fluorogenic assay, with sample fluorescence at endpoint reported as a function of initial substrate concentration for the Aβ derivative Mca-QKLVFFAEDVK(Dnp)-OH FRET peptide. **E.** Model for kinetic parameters of IDE function. Initial reaction velocity was determined for kinetic assays conducted in the presence of varying initial concentrations of Mca-VEALYLVCGEK(Dnp)-OH, as indicated. Kinetic parameters of IDE function including K_{half} and k_{cat} were derived from this data using the allosteric sigmoidal least squares nonlinear regression functionality of GraphPad PRISM v. 7.0. Average values from n=6 experimental replicates ± standard error of the mean are shown. **F.** Model for kinetic parameters of IDE function at varying initial concentrations of Mca-QKLVFFAEDVK(Dnp)-OH.

TABLE 1

Kinetic parameters of IDE proteolysis of insulin and Aβ peptide derivative FRET substrates.

Enzyme isolate	Mca-VEALYLVCGEK(Dnp)-OH			Mca-QKLVFFAEDVK(Dnp)-OH		
	Specific activity (nmol min^{-1} mg^{-1})	K_{half} (μM)	k_{cat} (min^{-1})	Specific activity (nmol min^{-1} mg^{-1})	K_{half} (μM)	k_{cat} (min^{-1})
WT IDE	116 ± 6	1.26 ± 0.14	11.9 ± 0.7	183 ± 12	3.16 ± 0.69	34.3 ± 4.4
E111Q	<1	-	-	<1	-	-
F115A	14 ± 1	-	-	158 ± 6	2.78 ± 1.08	43.5 ± 6.0
F115W	18 ± 1	-	-	129 ± 5	4.26 ± 1.50	43.9 ± 5.2
F115Y	54 ± 3	0.79 ± 0.58	12.0 ± 4.9	170 ± 8	4.12 ± 1.40	43.3 ± 5.2
F115N	28 ± 2	-	-	21 ± 3	-	-
F115D	4 ± 1	-	-	23 ± 2	-	-
F115K	<1	-	-	4 ± 1	-	-
A140F	<1	-	-	<1	-	-
A140W	<1	-	-	<1	-	-
A140Y	<1	-	-	<1	-	-
A140N	<1	-	-	<1	-	-
A140D	<1	-	-	<1	-	-
A140K	<1	-	-	<1	-	-
F141A	86 ± 2	2.68 ± 0.13	13.0 ± 0.6	85 ± 6	4.11 ± 1.20	19.8 ± 1.8
F141W	45 ± 1	4.26 ± 0.24	6.1 ± 0.5	221 ± 21	2.61 ± 0.70	37.5 ± 3.7
F141Y	105 ± 3	2.78 ± 0.06	10.7 ± 0.4	280 ± 17	3.26 ± 0.66	46.8 ± 3.9
F141N	63 ± 2	3.24 ± 0.08	7.4 ± 0.3	32 ± 2	-	-
F141D	29 ± 2	-	-	22 ± 2	-	-
F141K	35 ± 1	-	-	14 ±2	-	-
Y150F	96 ± 5	3.01 ± 0.13	13.3 ± 0.7	240 ± 19	4.51 ± 1.57	66.4 ± 9.0
Y150A	18 ± 4	-	-	33 ± 5	-	-
Y150W	55 ± 4	4.28 ± 0.15	8.6 ± 0.5	81 ± 6	5.94 ± 1.74	26.9 ± 2.7
Y150N	22 ± 1	-	-	34 ± 5	-	-
Y150D	27 ± 2	-	-	58 ± 2	-	-
Y150K	41 ± 2	3.14 ± 0.08	5.7 ± 0.3	72 ± 5	3.77 ± 0.68	17.9 ± 1.2
W199F	98 ± 4	2.51 ± 0.16	14.4 ± 0.8	66 ± 4	6.62 ± 2.03	20.3 ± 2.3
W199A	88 ± 6	3.16 ± 0.13	10.9 ± 0.5	21 ± 1	-	-
W199Y	78 ± 5	2.46 ± 0.10	9.4 ± 0.4	59 ± 4	3.08 ± 0.51	34.2 ± 2.1
W199N	84 ± 4	2.66 ± 0.11	10.6 ± 0.5	19 ± 1	-	-
W199D	18 ± 1	-	-	17 ± 1	-	-
W199K	53 ± 4	1.26 ± 0.13	5.3 ± 0.2	4 ± 2	-	-
F202A	35 ± 3	-	-	8 ± 1	-	-
F202W	83 ±4	2.32 ± 0.08	8.9 ± 0.3	167 ± 11	4.85 ± 0.82	48.2 ± 3.3
F202Y	130 ± 5	2.26 ± 0.10	14.6 ± 0.6	155 ± 5	2.65 ± 0.25	44.1 ± 1.8
F202N	78 ± 3	3.52 ± 0.05	10.3 ± 0.8	61 ± 5	-	-
F202D	64 ± 5	2.46 ± 0.06	5.8 ± 0.2	119 ± 2	2.46 ± 0.17	31.9 ± 0.9
F202K	56 ± 2	2.90 ± 0.09	5.8 ± 0.3	13 ± 1	-	-
F820A	7 ± 1	-	-	18 ± 3	-	-
F820W	130 ± 8	2.30 ± 0.20	9.6 ± 0.5	196 ±15	2.68 ± 0.51	50.8 ± 3.8
F820Y	93 ± 7	2.91 ± 0.09	6.5 ± 0.3	71 ± 10	2.71 ± 0.43	17.3 ± 1.0
F820N	9 ± 1	-	-	20 ± 1	-	-
F820D	<1	-	-	2 ± 1	-	-
F820K	3 ± 2	-	-	23 ± 2	-	-
Y831F	<1	-	-	<1	-	-
Y831A	<1	-	-	<1	-	-
Y831W	<1	-	-	<1	-	-
Y831N	<1	-	-	<1	-	-
Y831D	<1	-	-	<1	-	-
Y831K	<1	-	-	<1	-	-

Table 1. Kinetic parameters of IDE proteolysis of Mca-VEALYLVCGEK(Dnp)-OH or Mca-QKLVFFAEDVK(Dnp)-OH were determined for WT IDE, the IDE catalytic mutant E111Q (28), and other active site mutants described in this study. Kinetic parameters including the specific activity of IDE proteolysis at 20 μM initial substrate concentration, substrate concentration corresponding with half-maximal enzymatic activity (K_{half}), and maximal rate of substrate turnover (k_{cat}) are described. Average values from n=3 experimental replicates are reported ± standard error of the mean. For enzyme isolates that retained less than one third the specific activity of WT IDE, K_{half} and k_{cat} are not reported (-).

Conserved hydrophobic and aromatic residues of the IDE active site are critical to binding and proteolysis of insulin and Aβ derivative FRET peptides

Kinetic studies revealed that conserved hydrophobic and aromatic residues of the IDE active site are critical to proteolysis of insulin B chain and Aβ derivative FRET peptides (Table 1). A broad requirement for the conserved hydrophobic character of IDE active site residues was evident, as substitutions that introduced amino acid residues with hydrophilic or charged character were poorly tolerated. Notably, absolute conservation of IDE residues A140 and Y831 was essential to proteolytic activity, as all characterized substitutions introduced in place of either residue rendered the enzyme catalytically inactive. The absolute requirement for conservation of residue Y831 is in contrast with a prior study (23) that was conducted using the quenched fluorogenic peptide Substrate V (Mca-RPPGSFAFK(Dnp)-OH), a derivative of the inflammatory mediator bradykinin. Thus, the requirement for hydrophobic and aromatic IDE active site residues appears critically dependent on substrate identity.

A functional requirement for conservation of aromaticity of IDE active site residues was evident, as most mutagenic substitutions that introduced hydrophilic and/or charged amino acids in place of residues F115, F141, Y150, W199, F202 and F820 retained less than 20% of WT catalytic activity (Figure 3). Catalytically inactive IDE mutants were not subjected to further study using FRET peptides. However, mutants that retained at least 20% of WT IDE activity were subjected to analysis of kinetic parameters including evaluation of binding affinity (K_{half}) and turnover number (k_{cat}) towards insulin B chain and Aβ derivative FRET substrates (Table1). Among IDE active site mutants that retained substantial catalytic activity, most mutants that exhibited a lower rate of peptide substrate turnover also exhibited lower substrate binding affinity, suggesting that reduced substrate binding affinity may contribute to reduction in catalytic rate upon mutation of hydrophobic and aromatic IDE active site residues. Intriguingly, a number of hyperactive alleles of IDE, which exhibited increased rate of proteolysis of insulin B chain and Aβ derivative FRET peptides were also identified (i.e., Y150F, F202Y, and F820W; and F141Y, F141W, Y150F, F202W, F202Y, and F820W mutants, respectively; Table 1). Notably, all hyperactive IDE mutants preserved the native aromatic character of the mutagenized active site residues. Relative to the catalytic efficiency of WT IDE (10.85 ± 1.39 min^{-1} μM^{-1}) catalytic efficiency towards the Aβ derivative FRET substrate was most significantly increased for the F202Y mutant (16.96 ± 0.68 min^{-1} μM^{-1}, while more modest increases were observed for F141W (14.37± 1.42 min^{-1} μM^{-1}), F141Y (14.36 ± 1.20 min^{-1} μM^{-1}) and Y150F mutants (14.72 ± 2.00 min^{-1} μM^{-1}). Significant increases in catalytic efficiency towards the insulin B chain derivative FRET substrate were not observed among the mutants characterized.

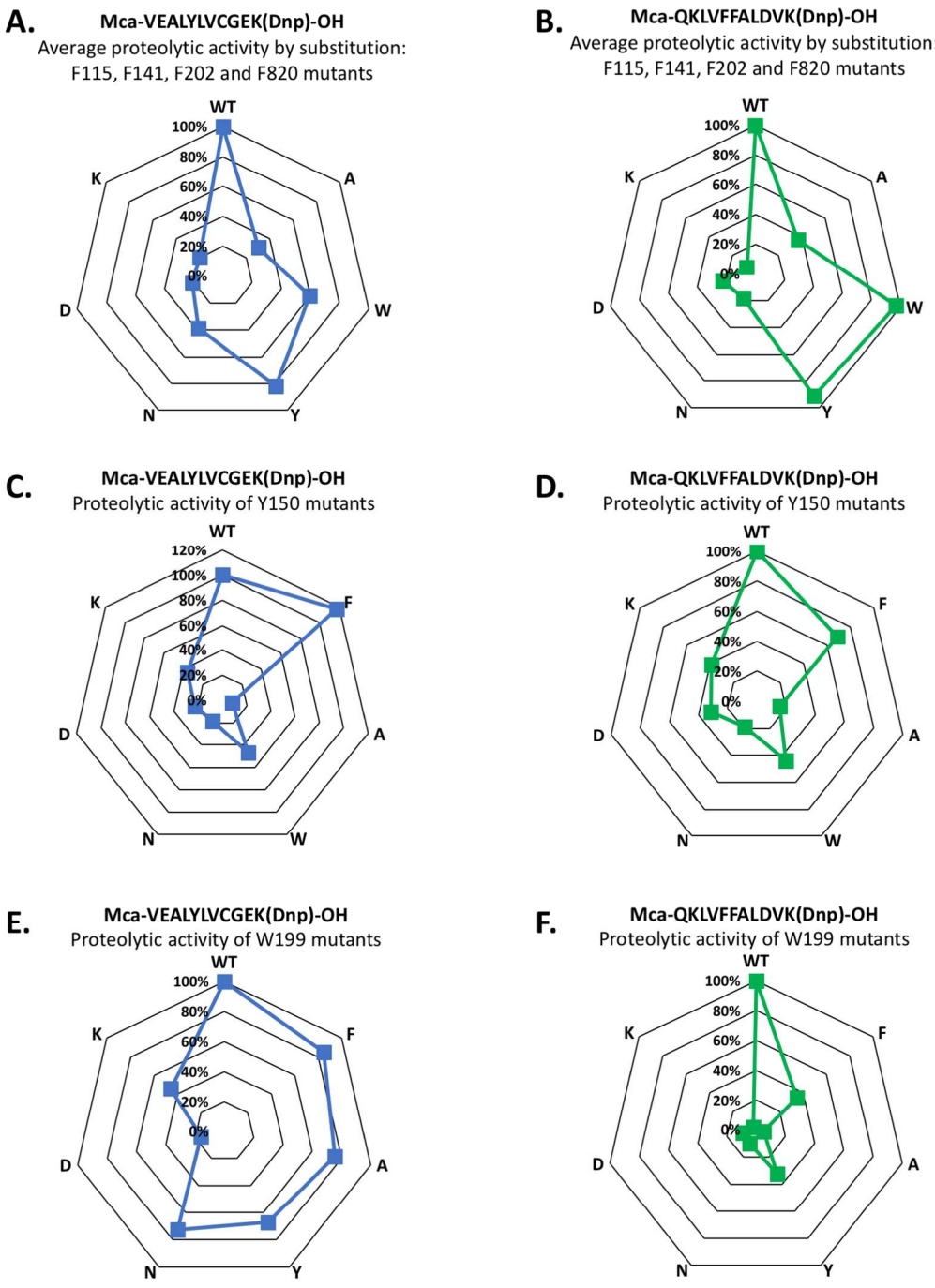

Figure 3. Aromaticity of IDE active site residues is critical for proteolysis. A. Average proteolytic activity of F115, F141, F202, and F820 mutants towards the insulin B chain derivative Mca-VEALYLVCGEK(Dnp)-OH peptide, by substitution. Radar graphs depict the relative specific activity of mutant enzymes by comparison to WT IDE. **B.** Average proteolytic activity of F115, F141, F202, and F820 mutants towards the Aβ derivative Mca-QKLVFFAEDVK(Dnp)-OH peptide, as a percentage of WT IDE activity, by substitution. **C.** Proteolytic activity of Y150 mutants towards Mca-VEALYLVCGEK(Dnp)-OH. **D.** Proteolytic activity of Y150 mutants towards Mca-QKLVFFAEDVK(Dnp)-OH. **E.** Proteolytic activity of W199 mutants towards Mca-VEALYLVCGEK(Dnp)-OH. **F.** Proteolytic activity of W199 mutants towards Mca-QKLVFFAEDVK(Dnp)-OH. The hydrophobicity of mutagenic substitutions decreases clockwise from top (WT) in each panel of the figure.

Hydrophobic and aromatic IDE active site residues direct proteolytic specificity towards insulin and Aβ 1-40

As IDE mutants bearing substitutions in residues A140 and Y831 were unable to cleave insulin and Aβ derivative FRET substrates, we examined whether these mutants were similarly inactive towards full-length insulin and Aβ 1-40. Proteolysis of full-length recombinant insulin (insulin-FITC) and Aβ 1-40 was examined using endpoint proteolysis assays that were evaluated by SDS-PAGE (Figure 4). By contrast with WT IDE, which exhibited proteolytic activity of approximately 2.3 ± 0.1 nmol min^{-1} mg^{-1} towards insulin-FITC and 6.9 ± 0.1 nmol min^{-1} mg^{-1} towards Aβ 1-40, the IDE E111Q catalytic mutant and both A140F and Y831F active site substitution mutants lacked observable proteolytic activity towards insulin-FITC (Figure 4A, 4C) and also towards Aβ 1-40 (Figure 4B, 4D). Thus, conservation of hydrophobicity, aromaticity, and high β-propensity of IDE active site residues appears critical to proteolysis of recombinant insulin and Aβ peptides in addition to FRET substrates.

Proteolysis of insulin-FITC and Aβ 1-40 by IDE mutants that exhibited only partial defects in proteolytic activity, including several mutants that exhibited apparent preference for cleavage of either insulin B chain or Aβ derivative FRET peptides, was similarly evaluated (Figure 5). IDE mutants that exhibited preferential cleavage of either insulin B chain or Aβ derivative FRET substrates were selected on the basis of their apparent differential specificity and further characterized using longer peptide substrates. IDE mutants that exhibited increased proteolytic selectivity towards insulin-FITC (F141W) and towards Aβ 1-40 (W199K) were identified.

By comparison with the ease of application of the reported FRET substrates for characterization of IDE activity, assays for measurement of insulin-FITC and Aβ 1-40 proteolysis by IDE offered more limited throughput and tractability and were accordingly more limited in scope. Not all mutants that exhibited increased selectivity towards insulin B chain or Aβ derivative FRET substrates exhibited increased specificity towards intact insulin-FITC and Aβ 1-40 (Fig. S9). Thus, IDE specificity determinants are not uniquely limited to the conserved hydrophobic and aromatic active site residues characterized in this study.

Functional analysis of the IDE substrate binding interface

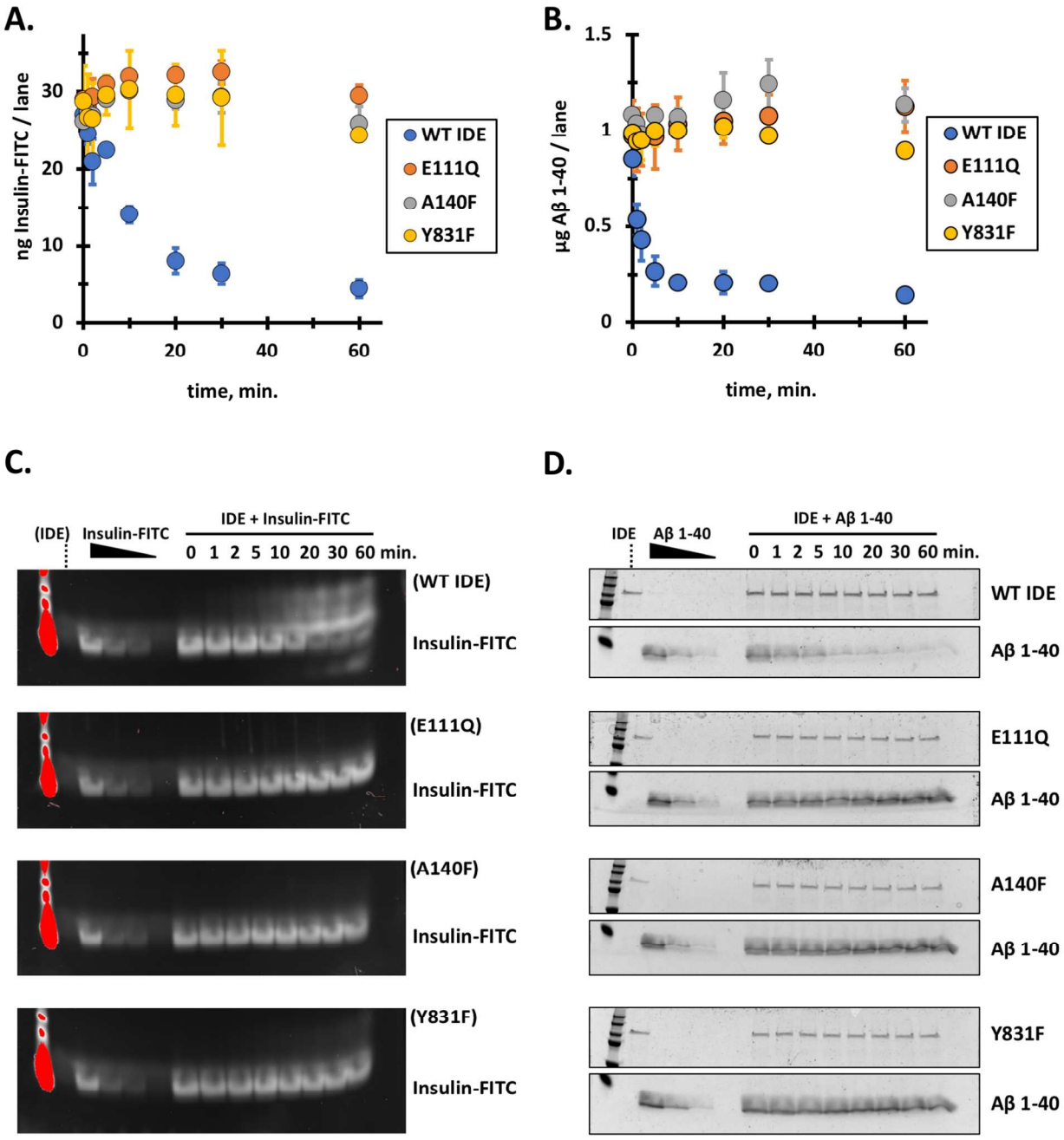

Figure 4. Hydrophobic and aromatic IDE active site residues are essential for proteolysis of insulin and Aβ 1-40. **A.** Densitometric analysis of insulin-FITC hydrolysis by WT IDE, E111Q, A1140F and Y831F mutants. The amount of insulin-FITC remaining at various intervals within the proteolytic time course was determined relative to internal standards for each experiment. Average values from n=2 experimental replicates ± standard error of the mean are shown. **B.** Densitometric analysis of Aβ 1-40 hydrolysis by WT IDE, E111Q, A1140F and Y831F mutants. The amount of Aβ 1-40 remaining at various intervals within the proteolytic time course was determined relative to internal standards for each experiment (below). **C.** Representative SDS-PAGE gels from the insulin-FITC proteolytic time course experiment. UV-transilluminated gel images are shown (20 s exposure; with fluorescein filter setting of Bio-Rad Gel Doc imaging system). Protein size marker and serially-diluted internal standards of 25 ng, 12.5 ng, 6.25 and 0 ng insulin-FITC are at positioned left, with proteolytic time course samples positioned towards the right of the gel. While present in the proteolytic experiment and where indicated as control, IDE does not exhibit significant fluorescence, and is not visible in the images shown. **D.** Representative Aβ 1-40 proteolytic time course experiment. Coomassie stained SDS-PAGE gel images are shown. Protein size marker and serially-diluted internal standards of 1 µg, 0.5 µg, 0.25 µg and 0 µg Aβ 1-40 are shown at left, with proteolytic time course positioned towards the right of the gel (bottom panels). IDE inputs are shown as control (top panels). Paired images are derived from the same SDS-PAGE gels.

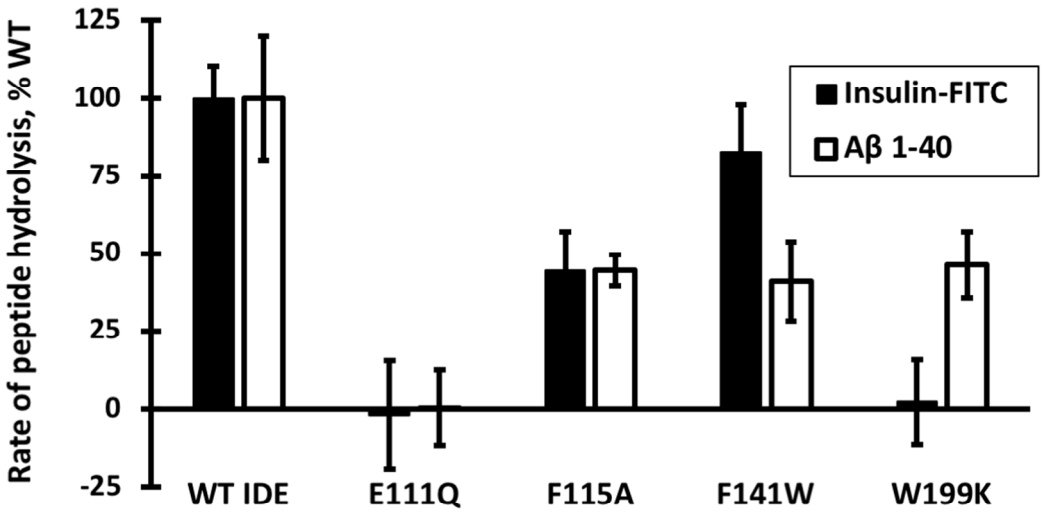

Figure 5. Substrate-selective IDE mutants. Relative rates of Insulin-FITC (black bars) and Aβ 1-40 (white bars) proteolysis by WT IDE and derivative mutants. Peptide hydrolysis was determined by densitometric analysis after a 5 minute proteolytic time course experiment relative to amounts of peptide hydrolyzed by WT IDE. Average values from n=2 experimental replicates are shown ± standard error of the mean.

DISCUSSION

This study demonstrates a critical role for conserved hydrophobic and aromatic residues of the IDE active site in the proteolysis of insulin, Aβ peptides, and fluorogenic peptide derivatives thereof. The functional significance of apolar IDE active residues is substrate-dependent and is influenced by both substrate length and primary sequence identity.

Several prior studies have examined the structure of the IDE active site (23) and peptide primary sequence determinants of IDE specificity (25, 26, 27). Shen et al. reported structural data for IDE in complex with insulin B chain (PDB ID 2G54), Aβ 1-40 (PDB ID 2G47) and other physiological substrates, which identified several hydrophobic surfaces of the enzyme in close proximity to bound substrates near ligands of the catalytic Zn^{2+} center (23). IDE substrates form β-sheets with IDE strand β6 (residues S137-S143) adjacent to the enzyme active site (23, 24), and form contact interfaces with residues of the α1 (G105-F115) and α5 (N196-N210) helices, as well as several residues from a conserved but unstructured loop (L823-Y831) of the IDE C-terminus.

IDE exhibits preference for substrates bearing basic or large hydrophobic amino acids near the site of IDE proteolytic cleavage but does not exhibit absolute substrate sequence requirements for peptide hydrolysis. Studies conducted using short fluorogenic synthetic peptides revealed that substrates which contain arginine, phenylalanine, leucine or tyrosine in the P1 or P1' subsites directly amino or carboxy terminal to the scissile peptide bond are cleaved with greatest catalytic efficiency (26, 34). IDE exhibits relative preference for efficient cleavage of substrates bearing aromatic or hydrophobic residues in the more distal P2, and to a lesser extent P2' subsites, consistent with the hypothesis that the enzyme contains an extended substrate binding site, and that IDE specificity is that is largely dictated substrate 3-dimensional structure (23, 27, 35). In addition, larger peptide substrates form binding interactions with IDE exosites located as much as 30 Å distal to the enzyme active site (23, 28, 29), in enzymatic regions that are not directly characterized in this study.

The structural models of Shen et al. (23), and functional models of Song et al. (27), Sefavi et al. (26), and others (24, 35) are broadly consistent with the findings from this study, which demonstrate a requirement for conservation of bulky hydrophobic and aromatic substrate binding residues of the IDE active site, including several regions that are important for the formation of β-structures. In addition, several specificity determinants of the IDE active site are characterized here.

First, IDE residues A140, F141 and Y150 collectively make up the proteolytic S1 subsite. Notably, these residues are contained on the β6 strand of IDE, which adopts β-structure interactions with various IDE substrates (24). The S1 subsite partially envelops bound substrates in the P1 position directly amino terminal to the hydrolyzed peptide bond. Functional conservation of the S1 subsite is critical to substrate binding and proteolysis, as introduction hydrophilic or charged aliphatic residues in place of residues A140, F141 and Y150 substantially attenuates IDE proteolytic activity and reduces binding affinity towards insulin B chain and Aβ peptide derivative FRET substrates.

Second, the IDE S1' subsite comprises residues F115, F820 and Y831. These residues are positioned in proximity to hydrophobic P1' residues of insulin B chain (L17) and Aβ 1-40 (F20). Residues of the IDE S1' subsite form a contact interface with bound substrates directly adjacent to the position of a common β-turn (23, 24). Together with the requirement for hydrophobic or aromatic residues in the S1 subsite, the requirement for hydrophobic and/or aromatic residues in the S1' position is consistent with a model in which IDE specificity is preferentially directed towards substrates bearing hydrophobic and aromatic amino acids directly adjacent to the scissile peptide bond (i.e., in the P1 and P1' positions) (27).

Third, an extended substrate binding site comprises at minimum residues W199 and F202 of the α5 helix of the IDE N-terminal subunit. Residue W199 is positioned within 4.5 Å of the P4, P3, and P2 substituents of insulin B chain (residues E13, A14, and L15) and Aβ 1-40 (residues K16, L17, and V18, respectively), and

together with residue F202 serves to cradle substrates in the P4 position near the boundary of defined substrate electron density in the crystal structures PDB ID 2G54 and PDB ID 2G47 (23). Conservation of the bulk, aromaticity and hydrophobicity of IDE residues W199 and F202 is critical to enzyme activity.

The functional requirement for IDE active site residues investigated here represents an important component of the broader model for IDE function, which must additionally account for extended substrate binding and mechanistic contributions much further removed from the enzyme active site. A more comprehensive model must therefore consider extended and potentially networked interactions occurring within the IDE allosteric (31) and exosites (28,29), which are not directly characterized here. Moreover, while all mutants characterized in this study were expressed with comparable yield and readily purified as proteins of the expected molecular mass (Fig. S1), we cannot rule out the possibility that introduced mutations may bring about a profound modification of the IDE active site micro-architecture which influences substrate specificity and kinetics of peptide hydrolysis.

Collectively, the findings from this study and others (23, 24, 25, 26, 27) support a model in which hydrophobic and aromatic residues of the IDE active site serve to limit or direct solvent accessibility during peptide hydrolysis by maintaining hydrophobic contacts, pi-stacking and β-structure interactions with bound substrates directly proximal to the scissile peptide bond. We speculate that the IDE active site residues characterized here play critical roles in the IDE catalytic mechanism by increasing the thermodynamic favorability of productive enzyme-substrate interactions, and by positioning bound peptide substrates in the appropriate orientation for proteolysis. By defining the characteristics of the IDE active site that are required for enzymatic specificity and proteolysis, this study contributes functional data informing the mechanism of action of IDE and related M16 proteases. This information may serve to guide therapeutic strategies for controlling IDE function through development of IDE inhibitors or substrate analogs targeting critical interactions within the enzyme active site, presenting intriguing opportunities for future research.

MATERIALS AND METHODS

Cloning, recombinant expression and purification of human IDE and derivative mutants

Human IDE was obtained much as previously described for related enzymes of the M16A subfamily (36, 37). The IDE gene characterized in this study was amplified from the GE Dharmacon™ cDNA library (product MHS6278-211689641 clone ID 40008464; GENBANK reference sequence BC096336) (38, 39). For bacterial expression, IDE was inserted from 5' to 3' at Nde1 and Xho1 cloning sites, respectively, in the pET-30b(+) expression vector (Novagen, Inc.) by gap cloning using the In-Fusion® HD cloning kit (Takara Bio Sciences).

Plasmid constructs directed expression of a C-terminal polyhistidine fusion protein bearing an N-terminal truncation relative to the BC096336 reference gene sequence (i.e., $IDE_{(M42\text{-}L1019)}$-6xHis). Derivative mutations were introduced by circular PCR amplification of the WT IDE expression construct using mutagenic oligonucleotides (Table S1). The WT IDE plasmid expression construct was validated by DNA sequencing throughout the full open reading frame, while derivative clones were validated across the site of mutation or truncation only (Keck DNA sequencing facility, Yale University; data not shown).

Bacterial cells (strain BL21 DE3) expressing WT IDE or derivative mutants were cultured in lysogeny broth supplemented with 50 μg/mL kanamycin antibiotic and induced for protein expression using 0.1 mM isopropyl β-D-1 thiogalactopyranoside (IPTG). Following induction, cultured cells were grown overnight at 25 °C, harvested by centrifugation, rinsed with phosphate buffered saline, and stored at -80 °C prior to cell lysis. Cell lysis was achieved by ultrasonic disruption, and cell lysates were clarified by centrifugation (3,200 g x 20 minutes at 4 °C). Clarified cell lysates were purified by nickel affinity chromatography using a Ni^{2+}-IDA resin in accordance with conditions recommended by the manufacturer (Takara Bio Sciences). Protein concentration was determined by Bradford assay prior to supplementation with glycerol and storage at -20 °C.

Development and application of insulin B chain and Aβ peptide derivative FRET substrates for kinetic studies of IDE proteolytic activity

Insulin B chain (Mca-VEALYLVCGEK(Dnp)-OH) and Aβ peptide derivative (Mca-QKLVFFAEDVK(Dnp)-OH) FRET substrates were developed as novel tools for the characterization of IDE proteolytic activity *in vitro*. FRET substrates were engineered to approximate the core regions of electron density for insulin B chain and Aβ 1-40 peptides at the IDE active site based on the available crystal structures (23). By comparison with established physiological substrates, FRET substrates used in this study comprised 5 amino acid residues N- and C-terminal to primary reported sites of IDE mediated cleavage of insulin B chain and Aβ 1-40 (23, 35, 40) flanked by N-terminal Mca fluorescing groups and C-terminal fluorescence-quenching K(Dnp) moieties.

Insulin B chain and Aβ peptide derivative quenched fluorogenic substrates (Mca-VEALYLVCGEK(Dnp)-OH and Mca-QKLVFFAEDVK(Dnp)-OH were synthesized using standard 9-fluorenylmoethyloxycarbonyl (Fmoc)-based chemistry with an Fmoc-Lys(Dnp) Wang resin on an automated peptide synthesizer (PS3, Gyros Protein Technologies, Inc.). The 7-methoxycoumarin-3-carboxylic acid was attached to each peptide backbone at the N-terminus using standard 2-(1H-benzotriazole-1-yl)-1,1,3,3-tetramethyl-uronium hexafluorophosphate (HBTU) coupling protocols. Peptides were cleaved from the resin using a cleavage cocktail of trifluoroacetic acid/ thioanisole/ethanedithiol/anisole (90/5/3/2) at room temperature for three hours. The peptides precipitated into ice-cold diethyl ether and were pelleted by centrifugation at 1300 x g for 10 minutes. The peptide pellets were then washed with diethylether and centrifuged two additional times.

FRET substrates were purified by reverse-phase HPLC (Shimadzu Prominence) with a Phenomenex Aeris Peptide C-18 semi-preparative column (150 x 10 mm) using a 3 mL/minute flow rate and a linear gradient of 60-80% and 45-65% acetonitrile over 15 minutes for Mca-VEALYLVGEK(Dnp)-OH and Mca-QKLVFFAEDK(Dnp)-OH peptides, respectively. The peptide product mass was confirmed by MALDI-TOF on a Shimadzu Axima Confidence mass spectrometer using α-cyano-4-hydroxycinnamic acid (CHCA) as matrix (Figure S3 and S4).

FMOC Lys(Dnp) Wang resin was purchased from Anaspec, Inc., and 7-methoxycoumarin-3-carboxylic acid was purchased from Chemodex, Inc. The FMOC protected amino acids, HBTU, deprotection solution, activating reagent, TFA, DMF and DCM were purchased from Gyros Protein Technologies, Inc. All other reagents were purchased from Fisher Scientific, Inc. Synthesis and purification of FRET substrates were further confirmed by mass spectrometric analysis of the HPLC purified peptides (Fig S3, S4).

Kinetic assays for IDE proteolysis of insulin and Aβ peptide derivative FRET substrates

To assess the role of IDE active site mutants in substrate binding and proteolysis, insulin B chain and Aβ peptide derivative FRET substrates were used to evaluate IDE activity in real time. For proteolysis assays to determine the specific activity of WT IDE and derivative mutants, a 50 μL reaction mixture was assembled containing 50 nM IDE and 20 μM of Mca-VEALYLVCGEK(Dnp)-OH or 25 nM IDE and 20 μM Mca-QKLVFFAEDVK(Dnp)-OH in a reaction buffer of 50 mM Tris(hydroxymethy) aminomethane, pH 7.3. To limit potential peptide aggregation, substrates were bath sonicated for 5 minutes at room temperature prior to assembling the enzymatic reaction mixture. Enzyme and substrate pre-mixtures were prepared independently and warmed to 37 °C prior to sample mixing and initiation of the proteolytic assay.

Fluorescence was measured using a Biotek Synergy HT plate reader (excitation: 325 ± 25 nm, emission: 420 ± 25 nm). Quantitative standardization of Mca-VEALYLVCGEK(Dnp)-OH and Mca-QKLVFFAEDVK(Dnp)-OH hydrolysis was achieved by determining fluorescence yield relative to known concentrations of Substrate V (Mca-RPPGFSAFK(Dnp), with linearity of fluorescence yield as function of product concentration established through the preparation of serially diluted peptide standards. To evaluate the functional consequences of IDE mutation with respect to substrate specificity and binding affinity, kinetic assays were conducted while varying initial substrate concentrations from 1.25-20 μM. Kinetic parameters including substrate concentrations that corresponded with half-maximal enzymatic activity (K_{half}; an approximation of binding affinity for allosteric enzymes) and maximal rate of substrate turnover (k_{cat}) were determined by non-linear regression using the allosteric sigmoidal least squares regression function ($Y = V_{max} \bullet X^h / (K_{half}^h + X^h)$, $X = [S]$) of the GraphPad PRISM 7 graphical analysis software.

FRET substrate proteolytic cleavage site mapping

To map IDE proteolytic cleavage sites within the internally quenched fluorogenic insulin B chain and Aβ derivative FRET substrates Mca-VEALYLVCGEK(Dnp)-OH and Mca-QKLVFFAEDVK(Dnp)-OH, 50 μL of a quenching solution containing 500 mM EDTA and 2% TFA were added to the 50 μL enzymatic assay mixtures at the midpoint of the proteolysis experiment. Samples were stored at -80 °C prior to analysis of peptide cleavage sites by MALDI-TOF mass spectrometry. A 25 μL aliquot of the quenched reaction mixture was prepared for MALDI-TOF mass spectrometry analysis with a C_{18} Reverse-Phase ZipTip® (Millipore) following manufacturer protocols. MALDI-TOF mass spectrometry analysis of FRET substrate IDE cleavage sites was mapped using CHCA MALDI matrix in reflectron mode and post-source decay MS/MS was conducted on major cleavage site peptide fragments (Axima Confidence, Shimadzu).

Mass spectrometric analysis of IDE proteolyzed Mca-VEALYLVCGEK(Dnp)-OH indicated a major cleavage site between the central tyrosine and leucine residues Y5 and L6 of the hendecameric peptide (Fig S5A and S5B). This site of hydrolysis is analogous to a major reported IDE cleavage site within insulin B chain, which is cleaved by IDE at the Y16 -L17 peptide bond and elsewhere (23, 41, 42). C-terminal post-source decay sequencing of this major peptide fragment confirmed the hydrolysis product as Mca-VEALY-OH (Figure S5C AND S5D). Mass spectrometric analysis of IDE proteolyzed Mca-QKLVFFAEDK(Dnp)-OH indicated a primary peptide cleavage site between the two central phenylalanine residues F5 and F6 (Figure S6A and S6B). This site of hydrolysis is analogous to a major reported IDE cleavage site within Aβ 1-40, which is cleaved by IDE at

the central F19-F20 peptide bond, as well as at other sites within the polypeptide (16, 23, 40, 43, 44). C-terminal post-source decay sequencing of the major peptide fragment confirmed the hydrolysis product as Mca-QKLVF-OH (Figure S6C and S6D).

Insulin and Aβ 1-40 proteolysis assays

To assess the impact of IDE active site mutations on proteolysis of intact insulin and Aβ 1-40, kinetic assays were conducted using purified recombinant peptides. IDE proteolysis assays were performed using labeled insulin (fluorescein isothiocyanate labeled recombinant human insulin peptide expressed in yeast, Sigma Aldrich Inc.) and unlabeled Aβ 1-40 peptides (HFIP-pretreated human recombinant peptide expressed in *E. coli*, rPeptide Inc.) and were evaluated by SDS-PAGE.

For insulin-FITC proteolysis experiments, enzymatic reactions contained 1.6 μg (180 nM) purified IDE and 400 ng (0.78 μM) insulin-FITC within an 80 μl reaction mixture buffered with 50 mM Tris, pH 7.3. For Aβ 1-40 proteolysis experiments, enzymatic reactions contained 4 μg (0.45 μM) IDE and 16 μg (45 μM) Aβ 1-40 within an 80 μl reaction mixture buffered with 50 mM Tris, pH 7.3. Enzyme and substrate pre-mixtures were initially prepared at 2X working concentration, and peptides were bath sonicated in reaction buffer prior to sample mixing to limit potential aggregation during the assay. Enzyme and substrate pre-mixtures were warmed before mixing. Proteolysis assays were conducted at 37 °C.

To terminate the proteolytic reaction, 5 μl aliquots were drawn from the assay mixtures at the time points indicated and transferred to 10 μl of an SDS-PAGE sample loading buffer/stop solution of 100 mM EDTA, 160 mM Tris, pH 6.8, 0.32% bromophenol blue, 32% glycerol and 160 mM β-mercaptoethanol. Thus inactivated, samples were held on ice for the remainder of the proteolytic experiment, then heated to 95 °C for 3 minutes directly prior to SDS-PAGE sample loading and analysis. An amount of the enzymatic reaction mixture equivalent to an initial substrate load of either 25 ng insulin-FITC or 1 μg Aβ 1-40 (i.e., for each time point, the entire proteolytic sample) was then input to individual wells of a Bio-Rad Any kDa™ TGX polyacrylamide gel and separated under denaturing conditions in the presence of a Tris-glycine SDS page running buffer. To limit background fluorescence, SDS-PAGE gels for insulin-FITC proteolysis experiments were pre-run at 150 V x 20 minutes prior to sample loading and electrophoretic separation.

Following electrophoresis (150 V x 45 min), SDS-PAGE gels for the insulin-FITC proteolysis assay were rinsed briefly with water (1-5 s), and immediately subjected to UV transillumination fluorescence imaging. SDS-PAGE gels for the Aβ 1-40 proteolytic assay were stained overnight using colloidal Coomassie Brilliant Blue™ G250 (45) and then destained for approximately 4 h prior to photographic scanning with white light transillumination. Quantitative densitometric analysis was performed using Bio-Rad Image Lab™ version 6.0 software. In each gel, internal standards from serial dilution of insulin-FITC or Aβ 1-40 were used to determine the amount of peptide remaining throughout the proteolytic assay.

ASSOCIATED CONTENT

Supporting information. Purification of IDE mutants, primary sequence conservation of IDE homologs, validation of synthesis and fluorogenic substrate cleavage site mapping, a comparison of kinetic models for IDE function, SDS-PAGE and densitometric data for insulin-FITC and Aβ 1-40 proteolysis assays, oligonucleotides for construction of IDE mutants, substrate interfacing IDE residues targeted for mutagenesis, and properties of free amino acids used for mutagenic substitution analysis are presented in the supporting information.

ACKNOWLEDGEMENT

We thank Dr. Brandon Lowe of St. Jude Children's Research Hospital and the reviewers of this manuscript for critical reading and constructive insights.

CONFLICT OF INTEREST

The authors declare that they have no conflicts of interest with the contents of this article.

AUTHOR CONTRIBUTIONS

L.S. performed and analyzed enzyme kinetic assays, and assisted protein purification and characterization. N.D.F. performed proteolytic digestion, and S.E.C. conducted MALDI mass spectrometric analysis mapping IDE cleavage sites in insulin and Aβ derivative FRET substrates. J.S.C. synthesized, purified and validated isolation of the internally quenched fluorescent peptides used in this study, and oversaw mapping their cleavage sites. B.J.A. conceived this study, cloned and purified IDE mutants, and coordinated organization of the manuscript.

FUNDING

This work was supported by the Department of Chemistry, College of Arts and Sciences, and award of University Research Creativity Grant funding from Sacred Heart University to BJA. This work was also supported by a grant from the U.S. National Science Foundation under CHE-1624774 to JSC.

REFERENCES

1. Mirsky, I. A.; Broh-Kahn, R. H. (1949) The inactivation of insulin by tissue extracts. I. The distribution and properties of insulin inactivating extracts insulinase. Arch. Biochem. 20, 1-9
2. Shii, K.; Yokono, K.; Baba, S.; Roth, R. A. (1986) Purification and characterization of insulin-degrading enzyme from human erythrocytes. Diabetes. 35, 675–683
3. Kirschner, R. J.; Goldberg, A. L. (1986) A high molecular weight metalloendoprotease from the cytosol of mammalian cells. J. Biol. Chem. (1983) 258, 967–976
4. Bennett, R. G.; Duckworth, W. C.; Hamel, F. G. Degradation of amylin by insulin-degrading enzyme. J. Biol. Chem. (2000) 275, 36621–36625
5. Kurochkin, I. V.; Goto, S. (1994) Alzheimer's beta-amyloid peptide specifically interacts with and is degraded by insulin degrading enzyme. FEBS Lett. 345, 33–37
6. Fakhrai-Rad, H.; Nikoshkov, A.; Kamel, A.; Fernström, M.; Zierath, J. R.; Norgren, S.; Luthman, H.; Galli, J. (2000) Insulin-degrading enzyme identified as a candidate diabetes susceptibility gene in GK rats. Hum. Mol. Genet. 9, 2149–58.
7. Karamohamed, S.; Demissie, S.; Volcjak, J.; Liu, C.; Heard-Costa, N.; Liu, J.; Shoemaker, C. M.; Panhuysen, C. I.; Meigs, J. B.; Wilson, P.; Atwood, L. D.; Cupples, L. A.; Herbert, A. (2003) Polymorphisms in the insulin-degrading enzyme gene are associated with type 2 diabetes in men from the NHLBI Framingham Heart Study. Diabetes. 52, 1562–1567
8. Farris, W.; Mansourian, S.; Chang, Y.; Lindsley, L.; Eckman, E. A.; Frosch, M. P.; Eckman, C. B.; Tanzi, R. E.; Selkoe, D. J.; Guenette, S. (2003) Insulin-degrading enzyme regulates the levels of insulin, amyloid beta-protein, and the beta-amyloid precursor protein intracellular domain in vivo. Proc. Natl. Acad. Sci. USA. 100, 4162–4167

9. Farris, W.; Mansourian, S.; Leissring, M. A.; Eckman, E. A.; Bertram, L.; Eckman, C. B.; Tanzi, R. E.; Selkoe, D. J. (2004) Partial loss-of-function mutations in insulin-degrading enzyme that induce diabetes also impair degradation of amyloid beta-protein. Am. J. Pathol. 164, 1425–1434
10. Tanzi, R. E.; Gusella, J. F.; Watkins, P. C.; Bruns, G. A.; St George-Hyslop, P.; Van Keuren, M. L.; Patterson, D.; Pagan, S.; Kurnit, D. M.; Neve, R. L. (1987) Amyloid beta protein gene: cDNA, mRNA distribution, and genetic linkage near the Alzheimer locus. Science. 235, 880–884
11. Hardy, J.; Allsop, D. Amyloid deposition as the central event in the aetiology of Alzheimer's disease. (1991) Trends Pharmacol. Sci. 12, 383–388
12. Hardy, J.; Selkoe, D. J. (2002) The amyloid hypothesis of Alzheimer's disease: progress and problems on the road to therapeutics. Science. 297, 353–356
13. Qiu, W. Q.; Walsh, D.M.; Ye, Z.; Vekrellis, K.; Zhang, J.; Podlisny, M. B.; Rosner, M. R.; Safavi, A.; Hersh, L. B.; Selkoe, D. J. (1998) Insulin-degrading enzyme regulates extracellular levels of amyloid beta-protein by degradation. J. Biol. Chem. 273, 32730–32738
14. Myers, A.; Holmans, P.; Marshall, H.; Kwon, J.; Meyer, D.; Ramic, D.; Shears, S.; Booth, J.; DeVrieze, F. W.; Crook, R.; Hamshere, M.; Abraham, R.; Tunstall, N.; Rice, F.; Carty, S.; Lillystone, S.; Kehoe, P.; Rudrasingham, V.; Jones, L.; Lovestone, S.; Perez-Tur, J.; Williams, J.; Owen, M. J.; Hardy, J.; Goate, A. M. (2000) Susceptibility Locus for Alzheimer's Disease on Chromosome 10. Science. 290, 2304–2305
15. Bertram, L.; Blacker, D.; Mullin, K.; Keeney, D.; Jones, J.; Basu, S.; Yhu, S.; McInnis, M. G.; Go, R. C.; Vekrellis, K.; Selkoe, D. J.; Saunders, A. J.; Tanzi, R. E. (2000) Evidence for genetic linkage of Alzheimer's disease to chromosome 10q. Science. 290, 2302–2303
16. Mukherjee, A.; Song, E.; Kihiko-Ehmann M.; Goodman, J. P. Jr.; Pyrek, J. S.; Estus, S.; Hersh L. B. (2000) Insulysin hydrolyzes amyloid beta peptides to products that are neither neurotoxic nor deposit on amyloid plaques. J. Neurosci. 20, 8745–8749
17. Leissring, M. A.; Selkoe, D. J. (2006) Structural biology: an enzyme target to latch on to. Nature. 443, 761–762
18. Selkoe, D. J. (2001) Clearing the brain's amyloid cobwebs. Neuron. 32, 177–180
19. Kurochkin, I. V. (2001) Insulin-degrading enzyme: embarking on amyloid destruction. Trends Biochem. Sci. 26, 421–425
20. Leissring, M. A.; Farris, W.; Chang, A. Y.; Walsh, D. M.; Wu, X.; Sun, X.; Frosch, M. P.; Selkoe, D. J. (2003) Enhanced proteolysis of beta-amyloid in APP transgenic mice prevents plaque formation, secondary pathology, and premature death. Neuron. 40, 1087–1093
21. Becker, A. B.; Roth, R. A. (1992) An unusual active site identified in a family of zinc metalloendopeptidases. Proc. Natl. Acad. Sci. USA. 89, 3835–3839
22. Rawlings, N. D.; Morton, F. R.; Kok, C. Y.; Kong, J.; Barrett, A. J. (2008) MEROPS: the peptidase database. Nucleic Acids Res. 36, D320–D325
23. Shen, Y.; Joachimiak, A.; Rosner, M. R.; Tang, W. J. (2006) Structures of human insulin-degrading enzyme reveal a new substrate recognition mechanism. Nature. 443, 870–874
24. Kurochkin, I. V.; Guarnera, E.; Berezovsky, I. N. (2018) Insulin-Degrading Enzyme in the Fight against Alzheimer's Disease. Trends Pharmacol. Sci. 39, 49–58
25. Authier, F.; Posner, B. I.; Bergeron, J.J. (1996) Insulin-degrading enzyme. Clin. Invest. Med. 19,149-160
26. Safavi, A.; Miller, B. C.; Cottam, L.; and Hersh, L. B. (1996) Identification of gamma-endorphin-generating enzyme as insulin-degrading enzyme. Biochemistry 35, 14318-14325
27. Song, E. S.; Mukherjee, A.; Juliano, M. A.; Pyrek, J. S.; Goodman, J. P. Jr.; Juliano, L., Hersh, L. B. (2001) Analysis of the subsite specificity of rat insulysin using fluorogenic peptide substrates. J. Biol. Chem. 276, 1152–1155

28. Tundo, G. R.; Di Muzio, E.; Ciaccio, C.; Sbardella, D.; Di Pierro, D.; Polticelli, F.; Coletta, M.; Marini, S. (2016) Multiple allosteric sites are involved in the modulation of insulin-degrading-enzyme activity by somatostatin. FEBS J. 283, 3755–3770
29. Malito, E.; Ralat, L. A.; Manolopoulou, M.; Tsay, J. L.; Wadlington, N. L.; Tang, W. J. (2008) Molecular bases for the recognition of short peptide substrates and cysteine-directed modifications of human insulin-degrading enzyme. Biochemistry. 47, 12822-12834
30. Zhang, Z.; Liang, W. G.; Bailey, L. J.; Tan, Y. Z.; Wei, H.; Wang, A.; Farcasanu, M.; Woods, V. A.;McCord, L. A.; Lee, D.; Shang, W.; Deprez-Poulain, R.; Deprez, B.; Liu, D. R.; Koide, A.; Koide, S.; Kossiakoff, A. A.; Li, S.; Carragher, B.; Potter, C. S.; Tang, W. J. (2018) Ensemble cryoEM elucidates the mechanism of insulin capture and degradation by human insulin degrading enzyme. eLife. 7, e33572
31. Im, H.; Manolopoulou, M.; Malito, E.; Shen, Y.; Zhao, J.; Neant-Fery, M.; Sun, C. Y.; Meredith, S. C.; Sisodia, S. S.; Leissring, M. A.; Tang, W. J. (2007) Structure of substrate-free human insulin-degrading enzyme IDE, and biophysical analysis of ATP-induced conformational switch of IDE. J. Biol. Chem. 282, 25453–25463
32. Perlman, R. K.; Gehm, B. D.; Kuo, W. L.; Rosner, M. R. (1993) Functional analysis of conserved residues in the active site of insulin-degrading enzyme. J. Biol. Chem. 268, 21538-21544
33. Perlman, R. K.; Rosner, M. R. (1994) Identification of zinc ligands of the insulin-degrading enzyme. J. Biol. Chem. 269, 33140–33145
34. Schechter, I.; Berger, A. (1967) On the size of the active site in proteases. I. Papain. Biochem. Biophys. Res. Commun. 27, 157–162
35. Duckworth, W. C.; Bennett, R. G.; Hamel, F. G. (1998) Insulin degradation: progress and potential. Endocr. Rev. 19, 608–624
36. Alper, B. J.; Rowse, J. W.; Schmidt, W. K. (2009) Yeast Ste23p shares functional similarities with mammalian insulin-degrading enzymes. Yeast. 26, 595–610
37. Smith-Carpenter, J. E.; Alper, B. J. (2018) Functional requirement for human pitrilysin metallopeptidase 1 arginine 183, mutated in amyloidogenic neuropathy. Protein Sci. 27, 861-873
38. Strausberg, R. L.; Feingold, E. A.; Grouse, L. H. ; Derge, J. G.; Klausner, R. D.; Collins, F. S.; Wagner, L.; Shenmen, C. M.; Schuler, G. D.; Altschul, S. F.; Zeeberg, B.; Buetow, K. H.; Schaefer, C. F.; Bhat, N. K.; Hopkins, R. F.; Jordan, H.; Moore, T.; Max, S. I.; Wang, J.; Hsieh, F.; Diatchenko, L.; Marusina, K.; Farmer, A. A.; Rubin, G. M.; Hong, L.; Stapleton, M.; Soares, M. B.; Bonaldo, M. F.; Casavant, T. L.; Scheetz, T. E.; Brownstein, M. J.; Usdin, T. B.; Toshiyuki, S.; Carninci, P.; Prange, C.; Raha, S. S.; Loquellano, N. A.; Peters, G. J.; Abramson, R. D.; Mullahy, S. J.; Bosak, S. A.; McEwan, P. J.; McKernan, K. J.; Malek, J. A.; Gunaratne, P. H.; Richards, S.; Worley, K. C.; Hale, S.; Garcia, A. M.; Gay, L. J.; Hulyk, S. W.; Villalon, D. K.; Muzny, D. M.; Sodergren, E. J.; Lu, X.; Gibbs, R. A.; Fahey, J.; Helton, E.; Ketteman, M.; Madan, A.; Rodrigues, S.; Sanchez, A.; Whiting, M.; Madan, A.; Young, A.C.; Shevchenko, Y.; Bouffard, G. G.; Blakesley, R. W.; Touchman, J. W.; Green, E. D.; Dickson, M. C.; Rodriguez, A. C.; Grimwood, J.; Schmutz, J.; Myers, R. M.; Butterfield, Y. S.; Krzywinski, M. I.; Skalska, U.; Smailus, D. E.; Schnerch, A.; Schein, J. E.; Jones, S. J.; Marra, M.A. (2002) Mammalian Gene Collection Program Team. Generation and initial analysis of more than 15,000 full-length human and mouse cDNA sequences. Proc. Natl. Acad. Sci. USA. 99, 16899–16903
39. Temple, G.; Gerhard, D. S.; Rasooly, R.; Feingold, E. A.; Good, P. J.; Robinson, C.; Mandich, A.; Derge, J. G.; Lewis, J.; Shoaf, D.; Collins, F. S.; Jang, W.; Wagner, L.; Shenmen, C. M.; Misquitta, L.; Schaefer, C. F.; Buetow, K. H.; Bonner, T. I.; Yankie, L.; Ward, M.; Phan, L.; Astashyn, A.; Brown, G.; Farrell, C.; Hart, J.; Landrum, M.; Maidak, B. L.; Murphy, M.; Murphy, T.; Rajput, B.; Riddick, L.; Webb, D.; Weber, J.; Wu, W.; Pruitt, K. D.; Maglott, D.; Siepel, A.; Brejova, B.; Diekhans, M.; Harte, R.; Baertsch, R.; Kent, J.; Haussler, D.; Brent, M.; Langton, L.; Comstock, C. L.; Stevens, M.; Wei, C.; van Baren, M. J.; Salehi-

Ashtiani K.; Murray, R. R.; Ghamsari, L.; Mello, E.; Lin, C.; Pennacchio, C.; Schreiber, K.; Shapiro, N.; Marsh, A.; Pardes, E.; Moore, T.; Lebeau, A.; Muratet, M.; Simmons, B.; Kloske, D.; Sieja, S.; Hudson, J.; Sethupathy, P.; Brownstein, M.; Bhat, N.; Lazar, J.; Jacob, H.; Gruber, C. E.; Smith, M. R.; McPherson, J.; Garcia, A. M.; Gunaratne, P. H.; Wu, J.; Muzny, D.; Gibbs, R. A.; Young, A. C.; Bouffard, G. G.; Blakesley, R. W.; Mullikin, J.; Green, E. D.; Dickson, M. C.; Rodriguez, A. C.; Grimwood, J.; Schmutz, J.; Myers, R. M.; Hirst, M.; Zeng, T.; Tse, K.; Moksa, M.; Deng, M.; Ma, K.; Mah, D.; Pang, J.; Taylor, G.; Chuah, E.; Deng, A.; Fichter, K.; Go, A.; Lee, S.; Wang, J.; Griffith, M.; Morin, R.; Moore, R. A.; Mayo, M.; Munro, S.; Wagner, S.; Jones, S. J.; Holt, R. A.; Marra, M. A.; Lu, S.; Yang, S.; Hartigan, J.; Graf, M.; Wagner, R.; Letovksy, S.; Pulido, J. C.; Robison, K.; Esposito, D.; Hartley, J.; Wall, V. E.; Hopkins, R. F.; Ohara, O.; Wiemann, S. (2009) Mammalian Gene Collection Program Team. The completion of the Mammalian Gene Collection MGC. Genome Res. 19, 2324–2333

40. Leissring, M. A.; Lu, A.; Condron, M. M.; Teplow, D. B.; Stein, R. L.; Farris, W.; Selkoe, D. J. (2003) Kinetics of amyloid β-protein degradation determined by novel fluorescence and fluorescence polarization-based assays. J. Biol. Chem. 278, 37314–37320
41. Grasso, G.; Rizzarelli, E.; Spoto, G. (2007) AP/MALDI-MS complete characterization of the proteolytic fragments produced by the interaction of insulin degrading enzyme with bovine insulin. J. Mass Spectrom. 42, 1590–1598
42. Duckworth, W. C.; Hamel, F. G.; Peavy, D. E.; Liepnieks, J. J.; Ryan, M. P.; Hermodson, M. A.; Frank, B. H. (1988) Degradation products of insulin generated by hepatocytes and by insulin protease. J. Biol. Chem. 263, 1826-1833
43. Morelli, L.; Llovera, R.; Gonzalez, S. A.; Affranchino, J. L.; Prelli, F.; Frangione, B.; Ghiso, J.; Castano, E. M. (2003) Differential degradation of amyloid beta genetic variants associated with hereditary dementia or stroke by insulin-degrading enzyme. J. Biol. Chem. 278, 23221–23226
44. Chesneau, V.; Vekrellis, K.; Rosner, M. R.; Selkoe, D. J. (2000) Purified recombinant insulin-degrading enzyme degrades amyloid beta protein but does not promote its oligomerization. Biochem. J. 351, 509–516
45. Candiano, G.; Bruschi, M; Musante, L.; Santucci, L.; Ghiggeri, G. M.; Carnemolla, B.; Orecchia, P.; Zardi, L.; Righetti, P. G. (2004) Blue silver: a very sensitive colloidal Coomassie G-250 staining for proteome analysis. Electrophoresis. 25, 1327–1333